

## Chapter 4

### Synthesis and characterization

In the preceding chapter the development of the indigenous FPGA-EMCCD system was described. This system combined the advantages of the high-end FPGA for precise control and implementation of the TL and OSL parameters along with the high-end capability of the EMCCD for image capturing. Spatial analysis of a very low level emission is possible using this instrument.

For the testing of this system nano scaled Calcium Fluoride was synthesized. As mentioned in the previous chapter the dose recovery tests done with this phosphor verified the proper working and the accuracy of the system. In order to compare this system with the standard commercially available systems of Risoe and Daybreak, the dose recovery tests were also done on them with the same phosphor and were found to be comparable as enumerated in chapter 3.

Along with the aim of testing the system, the nano scaled Calcium Fluoride was also synthesized with the propose of studying the phosphor. Since not much work has been done to understand the TL and OSL characteristics of a pure/un-doped nano sized phosphor, nano scaled Calcium Fluoride phosphor was synthesised and studied.

This and the next chapter deal with the synthesis and the characterization of this phosphor. For a holistic analysis of the phosphor, along with the study of TL and OSL characteristics, the structural and optical characterization of the phosphor is also done using XRD, PL and UV-Vis spectroscopy.

#### 4.1 Introduction

Calcium Fluoride ( $\text{CaF}_2$ ) is one of the earliest known thermoluminescent phosphor. Natural  $\text{CaF}_2$  has been extensively studied [1-6] for its thermoluminescence property and for its use in dosimetry. Though this phosphor is known to be very sensitive to light, not much has been

done to fully explore its OSL properties. This is the reason for the present study on synthetic  $\text{CaF}_2$ .

Nano sized materials have shown promising abilities. The change in the size of the constituent particle of the matter has a profound effect in the chemical and physical properties of the material. Calcium fluoride nano particles have great importance due to the many potential applications where it can be used [1]. The synthesis of nano  $\text{CaF}_2$  along with its optical and structural characterization is reported in this chapter.

Structural and optical characterization of the nano- $\text{CaF}_2$  gives important information about the sample. In the structural analysis, the crystallinity of the material, the size of its constituent grains and lattice constant is investigated using X-ray diffraction (XRD). In the optical analysis the characteristic absorption spectrum and emission spectrum is studied. For the optical absorption studies, Ultraviolet-Visible Spectroscopy (UV-Vis) and for emission studies Photoluminescence spectroscopy (PL) was used.

Nanomaterials are materials made up of crystallites or grains which are in the nanometer scale i.e. between 1 to 100 nm. At such a small size, they behave quite differently from their bulk material counterparts. Along with their size, they also have their own peculiar surface chemistry, shape and topology [2]. Due to the reduced particle size there are more atoms on the surface in a given amount of nanomaterial due to its increased surface to volume ratio [3]. This leads to more surface sites which changes the surface pressure and causes the change in the inter-particle spacing [4]. The lattice parameters and symmetry is changed due to the nano size of the particles. It causes instability in the atomic structure and the geometrical arrangements of the atoms change to give a modified structure. These effects bring large amount of changes in thermodynamic properties like melting point and so on.

The internal properties of material are also changed because the quantum confinement effect comes into play at this size. The phenomenon of electronic wave functions being influenced by size restrictions is called quantum confinement. If an electron is excited from the valence band to the conduction band of a semiconductor, leaving a hole in the valence band, the electron and hole can form a bound state through Coulomb interactions. This bound state has energy slightly less than the energy of the band gap. When the radius of a nanoparticle approaches the size of the exciton Bohr radius, the motion of the electrons and holes become confined in the nanoparticle. A created electron-hole pair can only fit into the nanoparticle when the charge carriers are in a state of higher energy. In this regime of spatial confinement

of the charge carriers, the kinetic energy becomes quantized and the energy bands will split into discrete levels. These phenomena are known as quantum size or quantum confinement effects. The confinement of a particle can be in zero dimension as bulk particle, one dimension known as quantum wells and three dimensions as nanoparticles.

Contrary to popular belief, the use of nanoparticles is not limited to the present times only. Nanoparticles were used for the metallic lustre decorations of the medieval ceramics. Metallic nanoparticles were used by the Romans for colouring glass [5]. Copper nanoparticles were found from Celtic red enamels dated from 400 to 100 B.C. [6]. Though nanoparticles were used since long, the people involved were not aware about it. It was only much later with the development of science and technology that the world of nano-materials came to light.

## **4.2 Synthesis of nano-CaF<sub>2</sub> by co-precipitation method**

The co-precipitation method was used for the synthesis of the phosphor. Tahvildari *et al* has reported this method to be effective for synthesis of nano materials with controllable size, uniform morphology and shape. It does not require higher temperatures and gives better homogeneity of the product [7].

Co-precipitation reactions involve the simultaneous occurrence of nucleation, growth, coarsening, and/or agglomeration processes. In the co-precipitation reactions the chemical reaction leads to supersaturating conditions necessary to induce precipitation. The products of precipitation reactions are generally sparingly soluble species formed under conditions of high super saturation. The conditions dictate that nucleation will be a key step of the precipitation process and that a large number of small particles will be formed. Secondary processes such as Ostwald ripening and aggregation, dramatically affect the size, morphology and properties of the products.

For a particular solvent, there is certain solubility for a solute, whereby addition of any excess solute will result in precipitation and formation of crystals. For nucleation to occur, the solution must be supersaturated either by directly dissolving the solute at higher temperature and then cooling to low temperatures or by adding the necessary reactants to produce a

supersaturated solution during the reaction [8, 9]. The precipitation process basically consists of a nucleation step followed by particle growth stages [10, 11].

There are three kinds of nucleation processes: homogeneous nucleation, heterogeneous nucleation and secondary nucleation. Homogeneous nucleation occurs in the absence of a solid interface by combining solute ions to produce nuclei. It happens due to the driving force of the thermodynamics because the supersaturated solution is not stable in energy. Uniformity of the size distribution is achieved through a short nucleation period that generates all of the particles obtained at the end of the reaction followed by a self sharpening growth process. The smaller particles grow more rapidly than the larger ones because the free energy driving force is larger for smaller particles than for larger ones if the particles are slightly larger than the critical size. Here focusing in size occurs.

Monodisperse size distribution can be obtained at this stage by either stopping the reaction (nucleation and growth) quickly or by supplying reactant source to keep a saturated condition. When the reactants are depleted due to particle growth, Ostwald ripening or defocusing will occur, where the larger particles continue to grow and the smaller ones get smaller and finally dissolve. Saturation ratio ( $S$ ) decreases now and the corresponding critical nuclei size increases. Therefore particles smaller than this new critical size will dissolve. If the reaction is quickly stopped at this stage, the particles will have a broad size distribution, which is featured by a distribution cantering two size regimes, a bigger one and a smaller one, and the critical size now at this saturation is in between. Once the reaction (mainly the growth of the particles) goes into this stage, it is difficult to get monodisperse particles unless the reaction is extended to long enough times to completely deplete the supersaturation and the smaller nuclei. The size of the particles gets relatively large and can extend into the micrometer size regime.

In addition to the growth by molecular addition where soluble species deposit on the solid surface, particles can grow by aggregation with other particles, and this is called secondary growth. The rate of particle growth by aggregation is much larger than that by molecular addition. After the particles grow to a stable size, they will grow by combining with smaller unstable nuclei and not by collisions with other stable particles.

Nano-sized  $\text{CaF}_2$  was synthesised using the co-precipitation method. The starting materials were anular grade (AR) calcium chloride ( $\text{CaCl}_2$ ) and ammonium fluoride ( $\text{NH}_4\text{F}$ ).  $\text{CaCl}_2$  and  $\text{NH}_4\text{F}$  were dissolved in two conical flasks containing 100 ml of distilled water in

stoichiometric proportions. Using a pipette  $\text{NH}_4\text{F}$  solution was added drop by drop to  $\text{CaCl}_2$  solution under vigorous stirring on a magnetic stirrer. The mixture was then stirred for 3 h constantly to achieve homogeneity. During stirring, the transparent reaction mixture transforms into opaque white suspension gradually. After 3 h stirring, the solution was centrifuged with ethanol for 15 min at 3000 rpm and at the end, white residue was obtained. The residue was washed thoroughly with absolute ethanol to remove the residual chloride and the ammonium ions. The final product was extracted on to a Petri dish and dried at room temperature. The size of the phosphor particles was calculated by Scherrer's formula using the XRD data.

### **4.3 Structural Characterization using XRD**

#### ***4.3.1 Theoretical background***

X-rays are a form of electromagnetic radiation that has high energies and short wavelengths of the order of the atomic spacing for solids. X-ray diffraction (XRD) was done to determine the size of the constituent grains and other structural properties. It is based on the phenomena of diffraction. Diffraction is the general characteristics of all waves and can be defined as the modification of the behaviour of light or other waves by their interaction with an object at the edge or corners. Diffraction also occurs when a wave encounters a series of regularly spaced obstacles that are capable of scattering the wave, and have spacing that is comparable in magnitude to the wavelength of the incident wave. Furthermore, diffraction is a consequence of specific phase relationships established between two or more waves that have been scattered by the obstacles [12, 13]. Considering an individual atom, if the beam of X rays is incident on the atom, the electrons in the atom absorb the energy and then oscillate about their mean positions. When an electron decelerates in its oscillations, it emits energy in the form of X-rays. This process of absorption and reemission of electromagnetic radiation is known as scattering. If the atoms are closely spaced, each of them contributes many scattered x-rays. The scattered waves from each atom interfere. If the waves are in phase constructive interference occurs. If the waves are  $180^\circ$  out of phase, then destructive interference occurs. A diffracted beam may be defined as a beam composed of large number of superimposed scattered waves. For a measurable diffracted beam complete destructive interference does not

take place. Thus diffracted beam is composed of a large number of scattered waves that mutually reinforce one another.

One of the most useful sources of information for crystal structure data is the powder diffraction file (PDF). It contains single phase X-ray diffraction patterns in the form of tables on inter-planar spacing and corresponding relative intensities. It also contains information like physical and crystallographic properties of the material. There was a committee constituted in 1969 known as Joint Committee on Powder Diffraction Standard (JCPDS) to collect standard diffraction patterns of material as repository. Later it was renamed as International Center for Diffraction Data (ICDD) in 1978. Both the acronyms JCPDS and ICDD are used to refer these patterns. The diffraction pattern obtained from diffractometer is compared with the standard patterns in the JCPDS-ICDD data base for matching of patterns and material identification. This matching is important for nanocrystalline materials that may contain several crystallographic phases, including highly disordered or amorphous phases and for nanocrystals whose crystal structure may be different from that of corresponding bulk form due to surface effects.

#### ***4.3.2 Instrumentation***

The three basic components of an x ray diffractometer are the x ray source, specimen, x ray detector and they all lie on the circumference of a circle, which is known as the focusing circle. The angle between the plane of the specimen and the x ray source is  $\theta$ , the Bragg angle. The angle between the projections of the x ray source and the detector is  $2\theta$ . For this reason, the X ray diffraction patterns produced with this geometry are often known as  $\theta$ - $2\theta$  scans. In the  $\theta$ - $2\theta$  geometry the x ray source is fixed, and the detector moves through a range of angles. The radius of the focusing circle is not constant but increases as the angle  $2\theta$  decreases. The  $2\theta$  measurement range is typically from  $0^\circ$  to about  $170^\circ$ . The choice of range depends upon the crystal structure of the material. For an unknown specimen a large range of angles is often used because the positions of the reflections are not known.

Although the  $\theta$  -  $2\theta$  geometry is the most common, there are other geometries. In the  $\theta - \theta$  geometry both the x-ray source and the detector move in the vertical plane in the opposite directions above the centre of the specimen. The other specialized techniques such as  $\omega$  scan and  $\phi$  scan are not widely used.

The diffractometer circle is different from the focusing circle. The diffractometer circle is centered at the specimen with the x-ray source and the detector on the circumference of the circle. The radius of the diffractometer circle is constant. The diffractometer circle is also called the Goniometer circle. The goniometer is the central component of an x-ray diffractometer and contains the specimen holder. It has arms to which the x-ray source and the detector are mounted. In most powder diffractometers, the goniometer is vertically mounted but in other diffractometers it may be horizontally mounted.

A standard x-ray diffraction pattern consists of a series of peaks whose intensity is plotted on y-axis and the measured diffraction angle  $2\theta$  along x-axis. These peaks are called reflections. Each reflection corresponds to x rays diffracted from specific set of planes in the specimen and these peaks are of different intensities. The intensity is proportional to the number of x ray photons of a particular energy that have been counted by the detector for each angle  $2\theta$ .

The intensities of reflections depend on several factors, including structure factor, incident intensity, slit width and the value of current and voltage used in the x ray source. The recorded x ray diffraction pattern generally has a background which is subtracted to smoothen the peaks. The intensity scale is often adjusted so as to have a reasonable intensity for all the peaks since the most intense peak may have a much higher intensity than the other peaks.

The structure and lattice parameters of the material are determined by the positions of the x ray diffraction peaks in the pattern. As the symmetry of the crystal structure decreases, there is an increase in the number of the peaks. The intensity of the reflections in a single phase material provides information about the atomic positions in the crystal.

### ***4.3.3 Results***

The phase identification, crystal structure, lattice parameters and particle sizes are determined by the powder XRD technique using a X'Pert Pro PANalytical powder diffractometer with Cu-K $\alpha$  radiation ( $\lambda = 1.54060 \text{ \AA}$ ) in the scan range 20-90°.

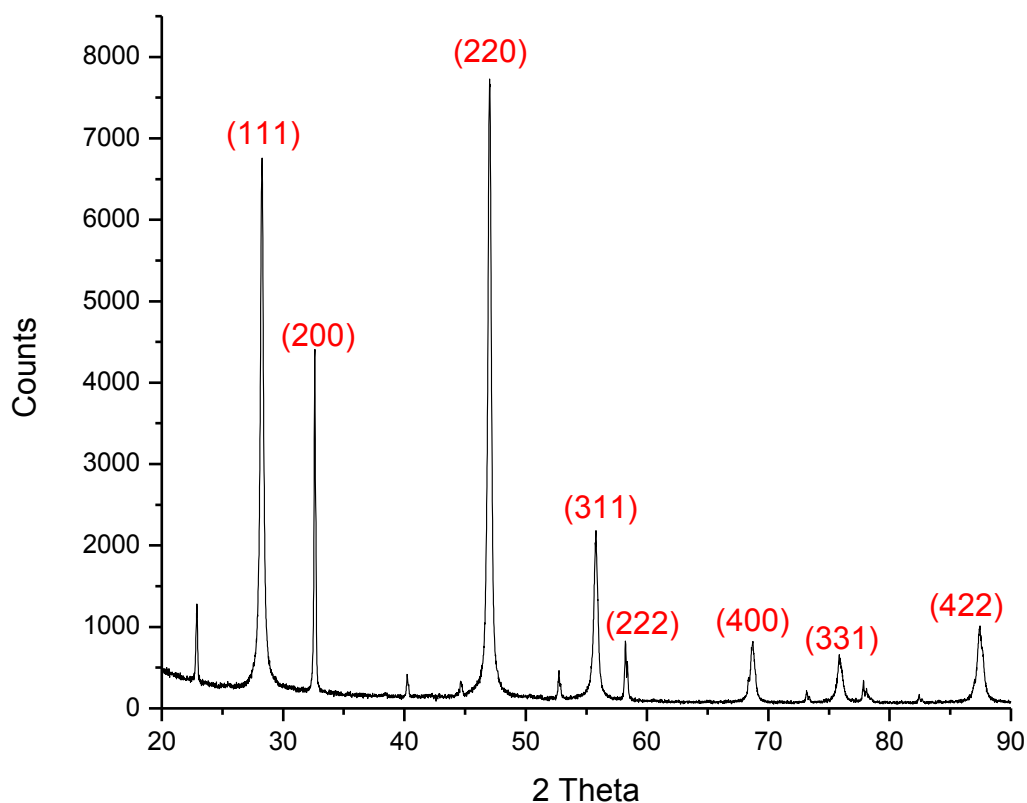


**Figure 1. Powder X-ray diffraction patterns**

All the obtained diffraction peaks were indexed and assigned to a cubic phase of the fluorite type structure with space group  $Fm\bar{3}m$ . The pattern was compared with JCPDS card no. 77-2245 and 75-0363. The diffraction patterns confirm the cubic crystallinity of the synthesized nanoparticles. The displayed peaks correspond to (hkl) values (111), (220), (311), (400), (311) and (422). The lattice constant  $a$  was calculated by using (hkl) values. The peak at (200) displays more intensity than found in the JCPDS card or in the literature. This could be due to the method of preparation. The average value of lattice constant was found to be 5.46868 Å for  $CaF_2$  nanocrystals. This is in close agreement with the value give in the literature [14, 15]. The crystallite size was calculated by Scherrer's formula and it was found to be 40.7 nm for  $CaF_2$  nanocrystals.

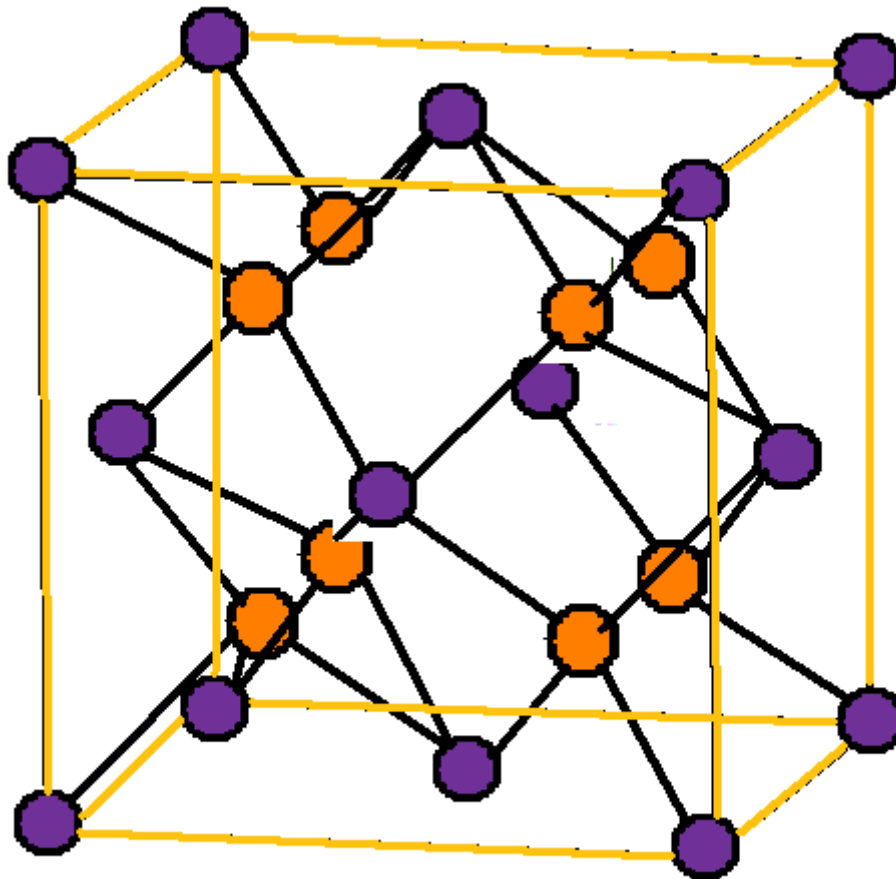


**Figure 2. Structure of CaF<sub>2</sub>**

The Scherrer's formula relates the size of sub-micrometre particles, or crystallites, in a solid to the broadening of a peak in a diffraction pattern. It is named after Paul Scherrer. The Scherrer equation is limited to nano-scale particles. It is not applicable to grains larger than about 0.1 to 0.2  $\mu\text{m}$ .

The Scherrer equation can be written as:

$$\tau = \frac{K\lambda}{\beta \cos\theta}$$

where:

$\tau$  is the mean size of the ordered (crystalline) domains, which may be smaller or equal to the grain size;

$K$  is a dimensionless shape factor, with a value close to unity. The shape factor has a typical value of about 0.9 but varies with the actual shape of the crystallite;

$\lambda$  is the X-ray wavelength;

$\beta$  is the line broadening at half the maximum intensity (FWHM), after subtracting the instrumental line broadening, in radians. This quantity is also sometimes denoted as  $\Delta(2\theta)$ ;

$\theta$  is the Bragg angle.

<b>2<math>\theta</math></b>	<b>FWHM</b>	<b>hkl</b>	<b>Crystallite Size d (nm)</b>	<b>Average d (nm)</b>
28.2314	0.277	111	30.875	40.70094
32.5976	0.117	200	73.85834	
46.9851	0.286	220	31.62153	
55.736	0.310	311	30.26524	
58.217	0.129	222	73.59006	
68.657	0.33	400	30.43498	
75.841	0.40	331	26.28506	
87.385	0.40	422	28.6773	

**Table 1. Calculation of Crystallite Size**

## **4.4 Optical characterization**

### **4.4.1 Ultra Violet/Visible Absorption Spectroscopy**

#### **4.4.1.1 Theoretical background**

The wavelength of light that a compound will absorb is characteristic of its chemical structure. Specific regions of the electromagnetic spectrum are absorbed by exciting specific types of molecular and atomic motion to higher energy levels. Absorption of microwave radiation is generally due to excitation of molecular rotational motion. Infrared absorption is associated with vibrational motions of molecules. Absorption of visible and ultraviolet (UV) radiation is associated with excitation of electrons to higher energy states in both atoms and molecules. For most molecules very high energy radiation is required (in the vacuum ultraviolet, <200 nm).

Absorption spectra measure the wavelength dependence of the intensity of light absorbed near the sample surface and in the bulk of the sample as well. By measuring absorption spectra, the absorbance of light energy by the sample can be obtained [16]. From the absorbance data, the energy bands of the material and the impurity levels within the material can be determined. Luminescence spectrum reveals only energy levels related to light emission. On the other hand absorption spectrum gives energy levels that may or may not be involved with light emitting transitions. Absorption spectra are characteristic of molecular structure and can be used to qualitatively identify atomic and molecular species.

The Beer-Lambert Law states that the concentration of a substance in solution is directly proportional to the 'absorbance', (A), of the solution.

$$A = \text{constant} \times \text{concentration} \times \text{cell length}$$

The law is only true for monochromatic light i.e. light of a single wavelength or narrow band of wavelengths, provided the physical or chemical state of the substance does not change with concentration.

When monochromatic radiation passes through a homogeneous solution in a cell, the intensity of the emitted radiation depends upon the thickness (L) and the concentration (C) of the solution.

The ratio  $I/I_0$  is called transmittance where  $I_0$  is the intensity of the incident radiation and  $I$  is the intensity of the transmitted radiation. This is sometimes expressed as a percentage and referred to as % transmittance. Mathematically, absorbance is related to percentage transmittance T by the expression

$$A = \log_{10} (I_0/I) = \log_{10} (100/T) = KCL$$

where L is the length of the radiation path through the sample, C is the concentration of absorbing molecules in that path and k is the extinction coefficient - a constant dependent only on the nature of the molecule and the wavelength of the radiation.

#### 4.4.1.2 Instrumentation

The measurement of Absorption spectra is done on UV-Vis Spectrophotometers [17]. The components include a radiation source, a monochromator to select the desirable wavelength of radiation to be examined, a sample container and a detector for measuring the intensity of radiation after it passes through the sample. The components can be lined up in two basic optical systems: (1) single-beam optics and (2) double- beam optics.

In the Single-beam optical system, radiation from the light source passes through the sample. From here the light proceeds to monochromator. The monochromator disperses the radiation in the same manner as a prism. By using a slit system with the monochromator, only light of the desired wavelength is allowed to proceed along the light path. This light passes to the detector. The detector in turn measures the intensity of the light, and the signal is read out on a recorder.

This system is subject to one major source of error. If the intensity of radiation from the source varies, then the entire signal drifts. The dual beam method is faster and has the advantage that lamp drift and other slow intensity fluctuations are properly accounted for in the calculation.

In the double-beam optical system, the light from the radiation source is split by a beam splitter and forms two paths, the reference path and the sample path. The beam splitting alternately directs the light from the radiation source along the reference path and then along the sample path. The light beams passing down these two paths are equal in intensity and pass alternately through sample and a reference. After passing through reference and sample, they are then recombined and continue through monochromator to the detector.

If there is no absorption by the sample or by the reference, then the two beams recombine to form the original un-split beam. This beam does not vary in intensity as the detector views alternately the reference beam and the sample beam. In this instance, the readout gives zero absorption.

### 4.4.1.3 Results

The optical absorption spectrum was recorded on a Thermo Scientific Evolution 600 UV-Visible spectrometer in a range 200-900 nm. The sample was dissolved in absolute ethanol and the absorbance was taken as a function of wavelength.

Optical absorption spectrum of  $\text{CaF}_2$  nanocrystals is given in figure 3. The absorption spectrum shows that characteristic absorption peak is present in the UV-region. The absorption peak observed in  $\text{CaF}_2$  nanocrystals is at 239 nm.

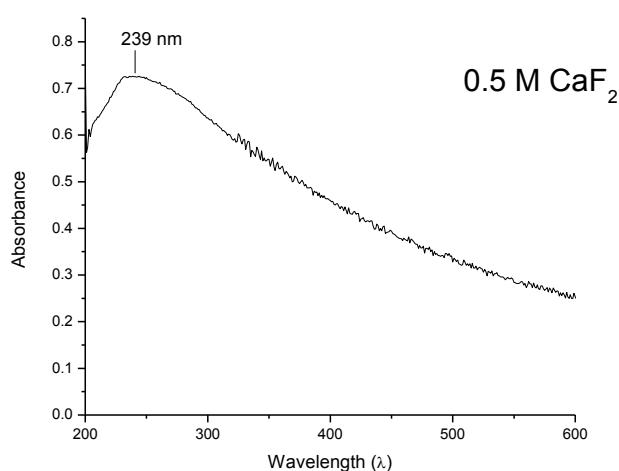


**Figure 3. Optical absorption spectrum of  $\text{CaF}_2$  nanocrystals**

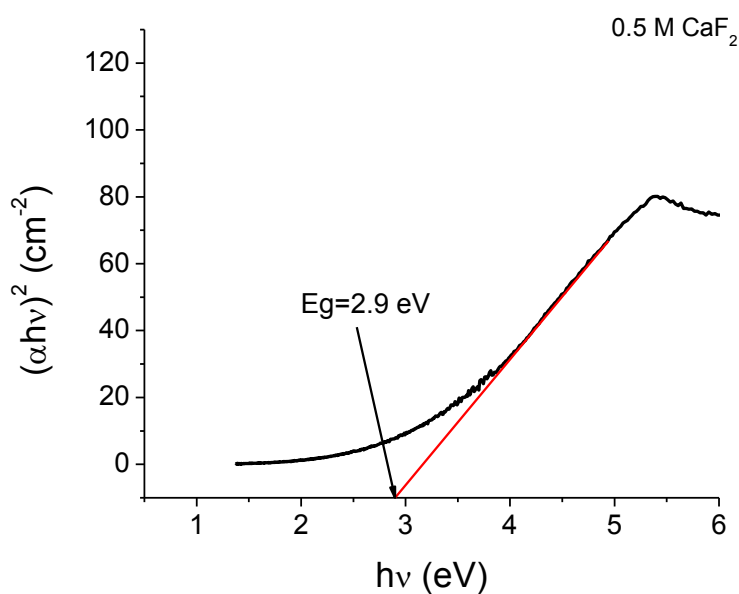


**Figure 4. Energy band gap plot of pure  $\text{CaF}_2$  nanocrystals**

The optical band gap energy ( $E_g$ ) was estimated by the method proposed by Wood and Tauc [18]. They proposed the following equation by which the optical band gap is associated with the absorbance and photon energy:

$$\alpha h\nu \propto (h\nu - E_g)^n$$

where

$h$  is the Planck constant,

$\nu$  is the frequency,

$\alpha$  is the absorbance,

$E_g$  is the optical band gap and

$n$  is a constant associated with different types of electronic transitions ( $n = 1/2, 2, 3/2$  or  $3$  for direct allowed, indirect allowed, direct forbidden and indirect forbidden transitions, respectively).

In order to find the band gap a Tauc plot is plotted which is graph of  $(\alpha h\nu)^2$  versus  $(h\nu)$ . The Tauc plot has a distinct linear region which indicates the beginning of absorption. Extrapolating this linear region to the x-axis gives the value of the band gap.

The energy band gap  $E_g$  was obtained from the optical absorption spectra by extrapolating the straight line plot of  $(\alpha h\nu)^2$  versus  $(h\nu)$  to the energy axis as shown in figure 4. Thus, the  $E_g$  value of the synthesised  $\text{CaF}_2$  nanocrystals was evaluated extrapolating the linear portion of the curve or tail. It was found to be 2.9 eV. This value is in agreement with the reported values in the literature [19]. For the bulk materials the band gap is around 12 eV. The values in literature ranges from 11.6 eV [20] to 12.1 eV [21]

## 4.4.2 Photoluminescence

### 4.4.2.1 Theoretical background

Photoluminescence refers to the emission of luminescence which is caused by the excitation of an electron in a crystal defect within the material due to absorption of light and then its subsequent return to the ground state emitting luminescence in the process. The intensity of this luminescence is directly proportional to the concentration of the defects in the material

where an electron can be excited due to the optical stimulation. The wavelength of this luminescence, according to Stokes' Law is equal to or longer than that of the exciting wavelength. In terms of energy, the emitted luminescence is of equal or less energy than that of the incident light. This difference in energy/wavelength is caused because the exciting light is transformed to a certain extent to non-radiating vibration energy of the constituent atoms or ions of the material. It is also possible that the emitted wavelength is shorter than the exciting wavelength or the energy of the emitted luminescence is more than that of the exciting light. This happens when thermal energy helps in the electron excitation process. The energy difference is called the anti-Stokes shift.

The phenomenon of photoluminescence is employed in Photoluminescence spectroscopy. A review of the photoluminescence spectroscopic techniques is given by Dean [23]. Using photoluminescence spectroscopy the electronic structures of materials can be investigated in a contactless, non-destructive, and non-invasive manner. Here light having higher energy than the band gap of the material under study is incident on the material. The incident light is partially reflected, absorbed, and transmitted by the sample. The absorbed photons are responsible for the excitation of electrons to the conduction band, or to the energy states within the forbidden gap, thus creating electron-hole pairs in the semiconductor. Electrons can also lose part of their energy and transfer from the conduction band to energy levels within the forbidden gap. The electrons and hole recombine emitting photons.

The intensity and spectral content of this emission (PL) is a direct measure of various important material properties. The photon energies point to the various energy states present in the material. The energy states are produced due to the various defects and due to the various manner in which the impurities are incorporated into the lattice. The recombination mechanism can also be inferred as the intensity of emission is related to the amount of radiative and non-radiative recombination.

#### **4.4.2.2 Instrumentation**

The instrument for PL has a stable and powerful monochromatic light source. A monochromator is also used in front of a light source for monochromatic excitation wavelength instead of a monochromatic light source. A detector is placed at 90° from the source axis. If it were placed in line with the source then along with emission it will detect the

excitation wavelength also. Due to this arrangement the cell containing the sample has two transparent faces perpendicular to each other. A monochromator is used in front of the detector to select the emission wavelength from the sample.

The light source has to be a source of high radiant power. Xenon arc lamp is generally used as the light source. The high radiant power of the xenon arc lamp makes them suitable for such applications. It produces an emission in the range from 200 nm to 1000 nm. Thus it covers the whole UV-Vis range. A high quality regulated power supply is needed to maintain consistency in the radiant power or else the emission from the sample will be affected. Lasers are also used as light source.

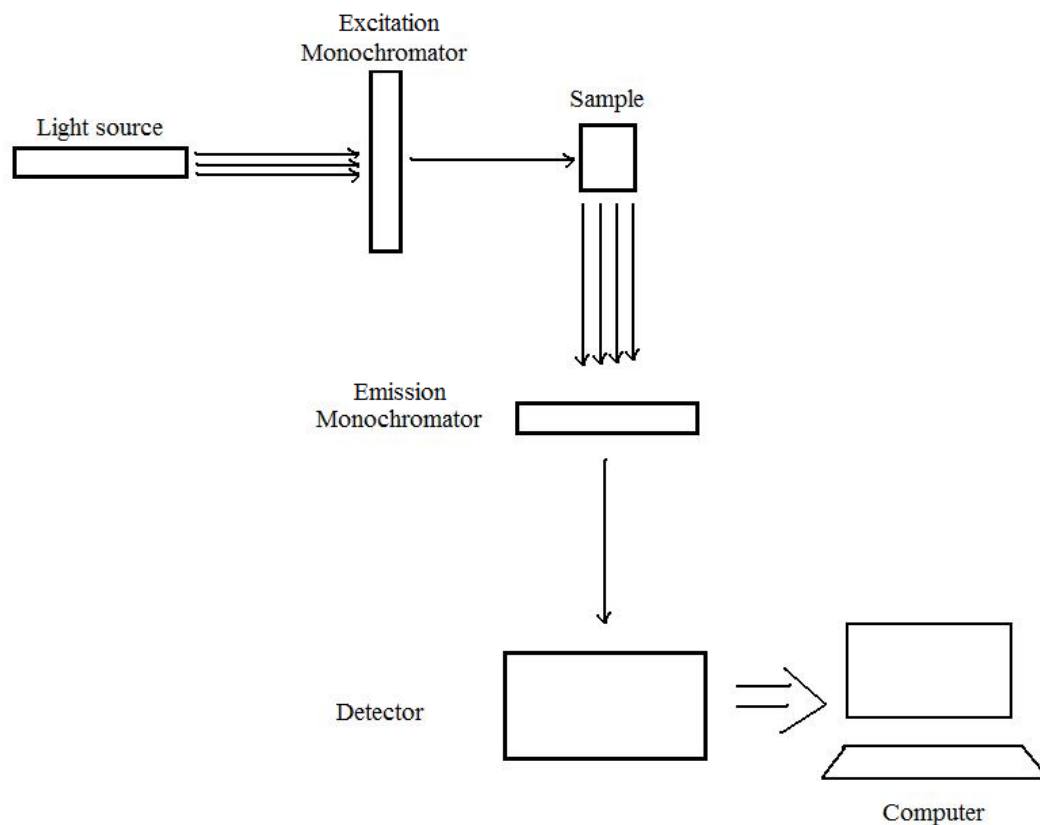


**Figure. 5 Schematic of PL instrument**

### 4.4.2.3 Results

The PL spectrum was carried out on a JASCO 6300 spectrophotometer.

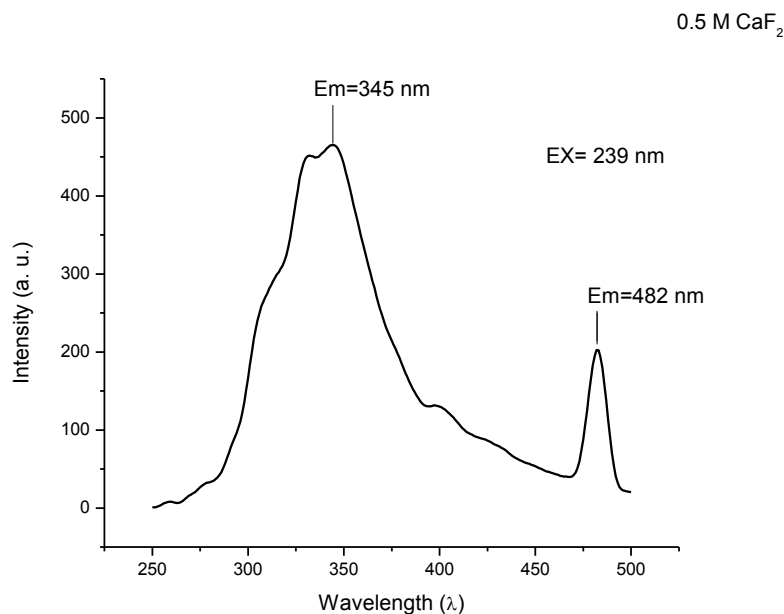


**Figure 6. PL emission spectrum of CaF<sub>2</sub> nanocrystals excited at 235 nm.**

Figure 6 shows the PL emission spectrum of CaF<sub>2</sub> for excitation at 239 nm. Broad emission was observed at 345 nm along with a small but distinct emission peak at 482 nm. These emission peaks can be attributed to self trapped exciton states [24]. The emission at 345 nm corresponds to an energy level of 3.59 eV calculated using the following formula.

$$E = \frac{hc}{\lambda}$$

where

E = energy in eV

h = Planck's constant which is  $4.13566751691 \times 10^{-15}$  eV . s

c = velocity of light which is 299792458 m/s

Similarly the emission peak at 482 nm corresponds to the energy level of 2.57 eV. The excitation wavelength of 239 nm is such that it has energy greater than the bandgap of the

material. The band-gap was found to be 2.9 eV by the UV spectroscopy described earlier. The 239 nm has the energy of 5.18 eV which is sufficient to excite all the electrons associated with the defects or the impurities in the material.

#### **4.5 Conclusion**

From the structural analysis it is confirmed that the material is calcium fluoride and by using Scherrer's formula the size of its constituent grains was found to be 40.7 nm.

From the optical analysis it is seen that the characteristic absorption peak of the material is present in the UV region. The absorption peak is at 239 nm. The optical band gap energy ( $E_g$ ) estimated by the method proposed by Wood and Tauc [18] was found to be 2.9 eV.

## References

- [1]. Omolfair, N., Nasser, S., Mahmood R., and Kompany, A., (2011). Synthesis and characterization of CaF<sub>2</sub> NPs with co-precipitation and hydrothermal method. *J Nanomedic Nanotechno*, 2, pp. 5
- [2]. Pradeep, T. (2007), *Nano the essentials—Understanding Nanoscience and Nanotechnology*, McGraw-Hill Education, India.
- [3]. Alivisatos, A. P., (1996). Perspectives on the Physical Chemistry of Semiconductor Nanocrystal, *J.Phy.Chem*, 100, pp. 13226.
- [4]. Goldstein, A. N., (1997) *Handbook of Nanophase Materials*, New York: Marcel Dekker, Inc.
- [5]. Sciau P. (2012). Nanoparticles in Ancient Materials: The Metallic Lustre Decorations of Medieval Ceramics, The Delivery of Nanoparticles, *InTech*, <http://www.intechopen.com/books/the-delivery-of-nanoparticles/nanoparticles-in-ancientmaterials-the-metallic-lustre-decorations-of-medieval-ceramics>
- [6]. Brun, N., Mazerolles, L., and Pernot, M., (1991). Microstructure of opaque red glass containing copper. *Journal of Materials Science Letters*, 10 (23), pp. 1418.
- [7] Tahvildari, K., Esmaeilipour, M., Ghammamy, S., and Nabipour H., (2012). CaF<sub>2</sub> nanoparticles: synthesis and characterization. *Int. J. Nano Dim.* 2 (4), pp. 269
- [8]. Peng, X., Wickham, J., and Alivisatos, A. P, (1998). *J. American Chemical Society*. 120, pp. 5343.
- [9]. Murray C. B., Kagan, C. R., and Bawendi, M. G., (2000). *Annual Review of Material Science* 30, pp. 545.
- [10]. Pamplin, B. R., (1975). *Crystal Growth*, New York: Pergamon Press.
- [11]. Jiang, Y., (2003) *Handbook of Nanophase and Nanostructured Materials*. New York: Kluwer Academic
- [12] Surnarayana, C., (1998). *X-Ray Diffraction - a practical approach*. New York: Grant Norton, Plenum press.

- [13] Heroll, P., and Alexander, L. E., (1954). *X-ray Diffracton Procedures for Polycrystalline and Amorphous Materials*. New York: John Wiley and Sons.
- [14] Shi, H., Eglitis, R. I. and Borstel G., (2005). First-principles calculations of the CaF<sub>2</sub> bulk and surface electronic structure. *phys. stat. sol. (b)* 242 (10), pp 2041
- [15] Johnson, E., and Chadderton, L.T., (1983). Anion voidage and the void superlattice in electron irradiated CaF<sub>2</sub>, *Rad. Effects* 79 pp. 183.
- [16] Shionoya S., and Yen, W. M., (1999) *Phosphor Handbook*. London: CRC press.
- [17] Robinson, J. W., (1975). *Atomic Absorption Spectroscopy* (2<sup>nd</sup> Ed), New York.
- [18] Wood D. L., and Tauc J., (1972) *Phys. Rev. B* 5, pp. 3144
- [19] Nakhaei, O., Shahtahmassebi, N., RezaeeroKnabadi, M., and Bagheri Mohagheghi, M.M. (2012) Synthesis, characterization and study of optical properties of polyvinyl alcohol/ CaF<sub>2</sub> nanocomposite films. *Scientia Iranica*, 19 (6), pp. 1979
- [20] Barth, J., Johnson, R.L., Cardona, M., Fuchs, D., and Bradshaw, A.M., (1990). Dielectric function of CaF<sub>2</sub> between 10 and 35 eV, *Phys. Rev. B* 41, pp. 291.
- [21] Rubloff, G.W., (1972). Far-ultraviolet reflectance spectra and the electronic structure of ionic crystals, *Phys. Rev. B* 5, pp. 662.
- [22] Dean, P.J., (1982). *Prog. Crystal Growth Charact.* 5, pp. 89.
- [23] Pandurangappa C, Lakshminarasappa BN (2011) Optical absorption and Photoluminescence studies in Gamma-irradiated nanocrystalline CaF<sub>2</sub>. *J Nanomedic Nanotechnol* 2:108. doi:10.4172/2157-7439.1000108